Supporting Information

Temperature-regulated biomass-derived hard carbon as superior anode for sodium-ion batteries

Figure Captions

Fig. S1 SEM images of (a) HC-1200, (b) HC-1400, and (c) HC-1600, respectively.

Fig. S2 peak fitting of the (002) peaks (a)HC-1000, (b)HC-1200, (c) HC-1400, (d) HC-1600, and (e) HC-2000.

Fig. S3 XPS spectra of the O1s: (a) HC-1000, (b) HC-1200, (c) HC-1400, (d) HC-1600, and (e) HC-2000, respectively.

Fig. S4 (a) Nitrogen adsorption-desorption isotherms and (b) BJH pore size distribution of HC-X samples.

Table S1 Physical parameters of N_2 adsorption-desorption and XPS.

Table S2 Electrochemical properties of the initial and second cycle of HC-X samples.

Fig. S5 Galvanostatic discharge/charge curves of HC-1400 paired with the $Na_3V_2(PO_4)_3$ cathode in coin type full cells at 0.1 C.

Table S3 Performance comparison of HC-1400 versus other biomass derived hard carbons of SIBs reported in literature.

Table S4 Performance comparison of hard carbon in this work versus other anodes of SIBs reported in literature.

Fig. S6 Galvanostatic intermittent titration curve vs. time of HC-1400 electrode.

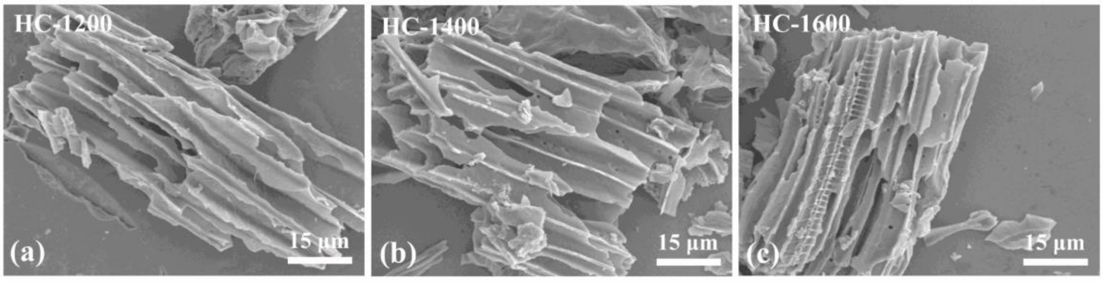

Fig. S1 SEM images of (a) HC-1000, (b) HC-1200, (c) HC-1400, and (d) HC-1600, respectively.

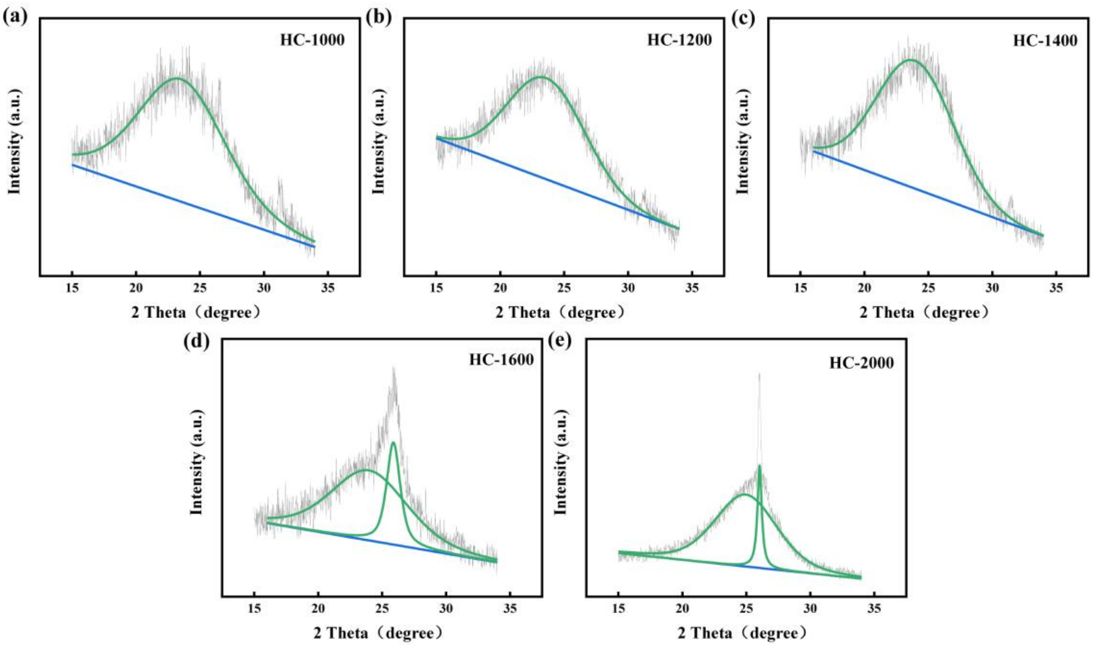

Fig. S2 peak fitting of the (002) peaks (a) HC-1000, (b) HC-1200, (c) HC-1400, (d) HC-1600, and (e) HC-2000.

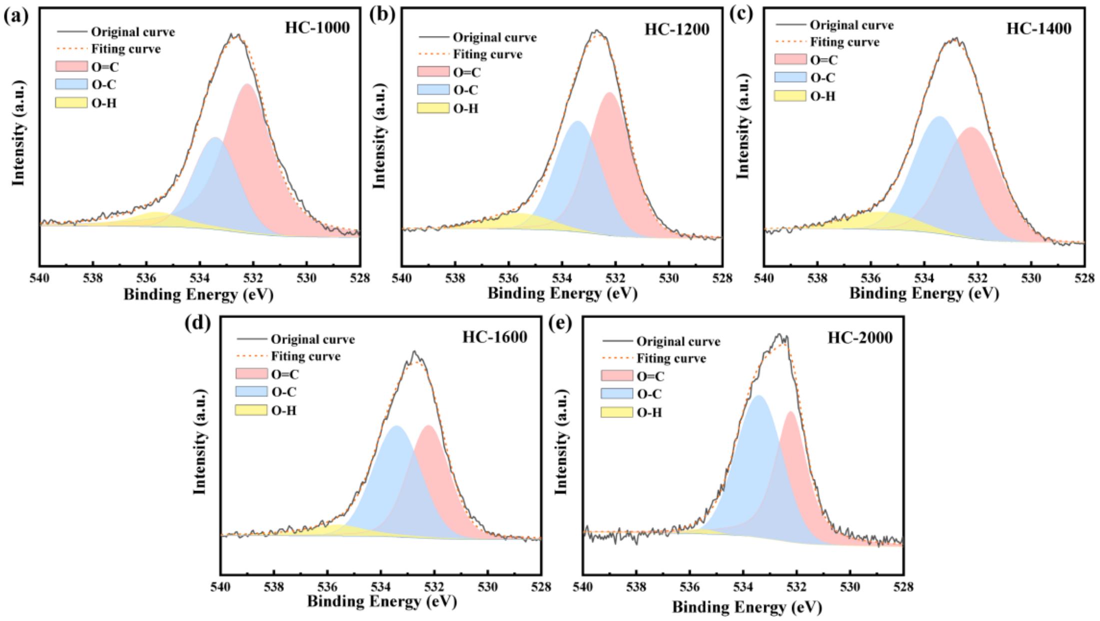

Fig. S3 XPS spectra of the O1s: (a) HC-1000, (b) HC-1200, (c) HC-1400, (d) HC-1600, and (e) HC-2000, respectively.

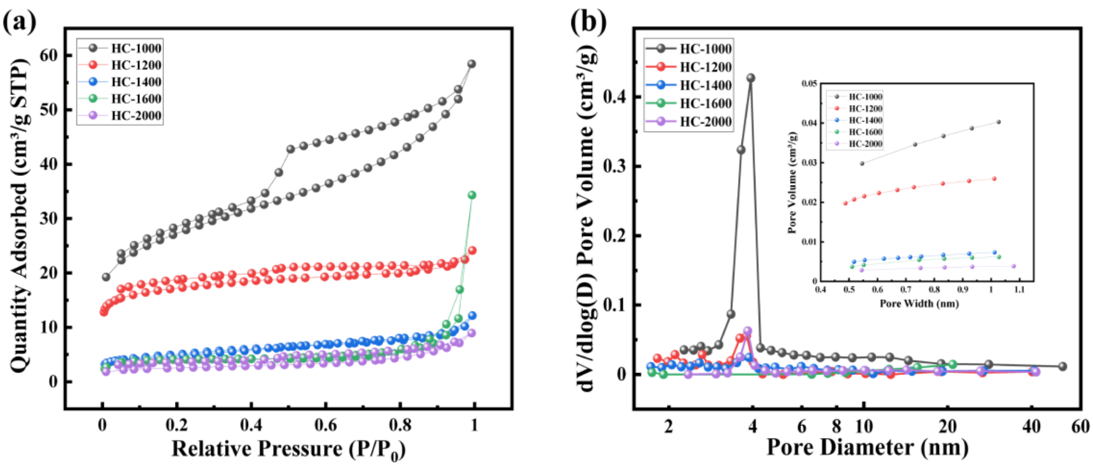

Fig. S4 (a) Nitrogen adsorption-desorption isotherms and (b) BJH pore size distribution of HC-X samples.

Table S1 Physical parameters obtained by N_2 adsorption-desorption and XPS.

Samples	N_2 adsorption-desorption				XPS	
	BET surface area (m^2 g^{-1})	Total pore volume (cm^3 g^{-1})	Micropore volume (cm^3 g^{-1})	Pore diameter (nm)	C at%	O at%
HC-1000	93.25	0.090	0.020	5.15	93.08	6.92

HC-1200	54.04	0.037	0.018	4.46	94.46	5.54
HC-1400	17.34	0.019	0.018	5.74	94.81	5.19
HC-1600	11.99	0.013	0.005	12.81	94.99	5.01
HC-2000	8.58	0.013	0.002	11.22	97.67	2.33

Table S2 Electrochemical properties of the first and second cycle of HC-X samples.

Samples	ICE (%)	1^{st} DC[a] (mA h g^{-1})	1^{st} CC[b] (mA h g^{-1})	2^{nd} slope capacity (mA h g^{-1})	2^{nd} plateau capacity (mA h g^{-1})	Proportion of plateau capacity (%)
HC-1000	74.38	320.7	238.5	121.3	122.7	50.28
HC-1200	79.62	308.6	245.7	97.2	156.1	61.63
HC-1400	86.43	338.7	292.7	83.0	214.2	72.07
HC-1600	77.01	340.5	262.2	50.3	209.7	80.65
HC-2000	81.35	256.9	209.0	19.42	199.0	91.11

[a] discharge capacity; [b] charge capacity.

Table S3 Performance comparison of HC-1400 versus other biomass derived hard carbons of SIBs reported in literature.

Biomass precursor	ICE (%)[a]	ICC (mA h g^{-1})[b]	CD (mA g^{-1})[c]	CT (°C)[d]	Raferences
golden berry leaves	86.4%	292.7	20	1400	This work
pine pollen	59.8%	221.5	100	900	[1]
cherry petals	67.3%	310.2	20	1000	[2]
Kelp	59.5%	273	25	1300	[3]
Algal Blooms	52.1%	231.1	20	1000	[4]
coconut endocarp	65.2%	246.7	50	1100	[5]
corncob	30.9%	152	100	700	[6]
garlic peel	41%	258	100	850	[7]
dandelion	51.8%	136.32	50	1400	[8]

[a] Initial Coulomb efficiency; [b] Initial charge capacity (mA h g^{-1}); [c] Current density; [d] Carbonization temperature

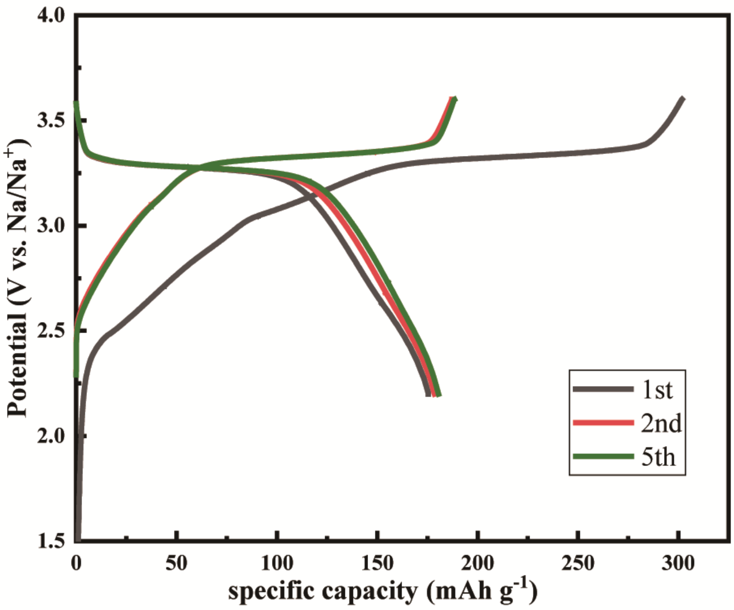

Fig. S5 Galvanostatic discharge/charge curves of HC-1400 paired with the $Na_3V_2(PO_4)_3$ cathode in coin type full cells at 0.1 C.

Table S4 Performance comparison of hard carbon in this work versus other anodes of SIBs reported in literature.

Materials	Potential (V)	ICE (%)	Capacity (mAh g^{-1})	Current Density (mA g^{-1})	Ref
HC-1400	0.01-2.0	86.4	292.7	20	This work
Porous Sn	0.01–1.0	60	519	424	[9]
Sb@C	0.001–2.0	69	371	500	[10]
$P@Ti_3C_2$	0.005–3.0	80	230	100	[11]
Red P	0.01-2.0	79.6	737	100	[12]
$Na_2Ti_3O_7$	0.1–2.5	36	221	35.4	[13]
TiO/MoS_2-NFs	0.01-3.0	84.6	676	100	[14]
SnS_2	0.01–3.0	55	680	200	[15]

Bi/Sb	0.01–2.0	69	550	200	[16]
GeP/rGO	0.01-2.5	57	620	100	[17]
MoS_2/Graphene	0.01–2.8	52	432	100	[18]
Nb_2O_5@S-rGO	0.01–3.0	35	325	100	[19]
$Ti_3C_2T_x$	0.01–3.0	53.8	295	500	[20]
$MoS_2/Ti_3C_2T_x$	0.01–3.0	69	250.9	100	[21]
Graphite	0.01–2.5	55	127	100	[22]
Soft carbon	0.01–3.0	40	200	50	[23]
graphene	0.01–2.8	62	255	100	[24]

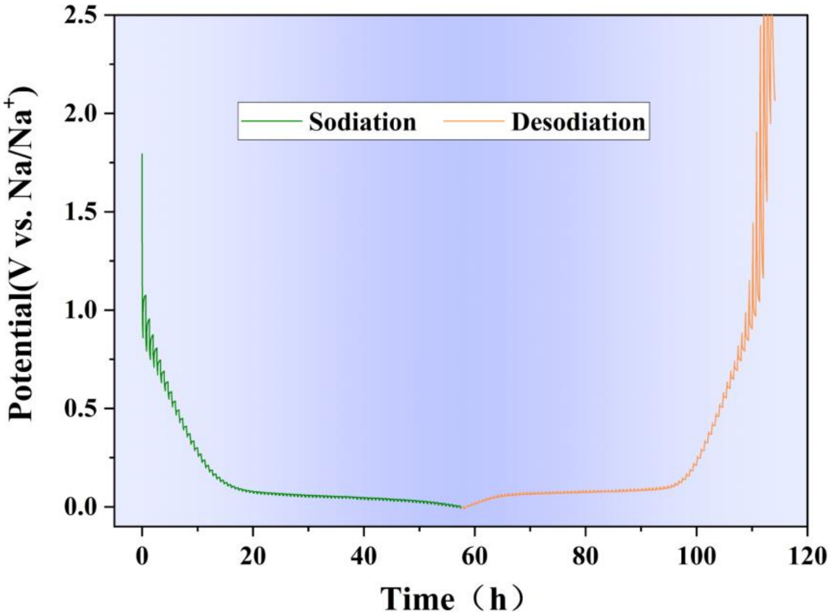

Fig. S6 Galvanostatic intermittent titration curve vs. time of HC-1400 electrode.

References

[1] Y. J. Zhang, X. Li, P. Dong, G. Wu, J. Xiao, X. Y. Zeng, Y. J. Zhang and X. L. Sun, Honeycomb-like Hard Carbon Derived from Pine Pollen as High-Performance Anode Material for Sodium-Ion Batteries, *ACS Appl. Mater. Interfaces*, 2018, **10**, 42796-42803.

[2] Z. Y. Zhu, F. Liang, Z. R. Zhou, X. Y. Zeng, D. Wang, P. Dong, J. B. Zhao, S. G.

Sun, Y. J. Zhang and X. Li, Expanded biomass-derived hard carbon with ultrastable performance in sodium-ion batteries, *J. Mater. Chem. A.*, 2018, **6**, 1513-1522.

[3] P. Z. Wang, X. S. Zhu, Q. Q. Wang, X. Xu, X. S. Zhou and J. C. Bao, Kelp-derived hard carbons as advanced anode materials for sodium-ion batteries, *J. Mater. Chem. A.*, 2017, **5**, 5761-5769.

[4] X. H. Meng, P. E. Savage and D. Deng, Trash to Treasure: From Harmful Algal Blooms to High-Performance Electrodes for Sodium-Ion Batteries, *Environ. Sci. Technol.*, 2015, **49**, 12543-12550.

[5] F. Wu, L. Liu, Y. F. Yuan, Y. Li, Y. Bai, T. Li, J. Lu and C. Wu, Expanding Interlayer Spacing of Hard Carbon by Natural K^+ Doping to Boost Na-Ion Storage, *ACS Appl. Mater. Interfaces*, 2018, **10**, 27030-27038.

[6] Q. Jiang, Z. H. Zhang, S. Y. Yin, Z. P. Guo, S. Q. Wang and C. Q. Feng, Biomass carbon micro/nano-structures derived from ramie fibers and corncobs as anode materials for lithium-ion and sodium-ion batteries, *Appl. Surf. Sci.*, 2016, **379**, 73-82.

[7] V. Selvamani, R. Ravikumar, V. Suryanarayanan, D. Velayutham and S. Gopukumar, Garlic peel derived high capacity hierarchical N-doped porous carbon anode for sodium/lithium ion cell, *Electrochim. Acta.*, 2016, **190**, 337-345.

[8] C. W. Wang, J. F. Huang, H. Qi, L. Y. Cao, Z. W. Xu, Y. Y. Cheng, X. X. Zhao and J. Y. Li, Controlling pseudographtic domain dimension of dandelion derived biomass carbon for excellent sodium-ion storage, *J. Power Sources*, 2017, **358**,

85-92.

[9] C. Kim, K. Y. Lee, I. Kim, J. Park, G. Cho, K. W. Kim, J. H. Ahn and H. J. Ahn, Long-term cycling stability of porous Sn anode for sodium-ion batteries, *J. Power Sources*, 2016, **317**, 153-158.

[10] J. Duan, W. Zhang, C. Wu, Q. J. Fan, W. X. Zhang, X. L. Hu and Y. H. Huang, Self-wrapped Sb/C nanocomposite as anode material for High-performance sodium-ion batteries, *Nano Energy*, 2015, **16**, 479-487.

[11] R. J. Meng, J. M. Huang, Y. T. Feng, L. H. Zu, C. X. Peng, L. R. Zheng, L. Zheng, Z. B. Chen, G. L. Liu, B. J. Chen, Y. L. Mi and J. H. Yang, Black Phosphorus Quantum Dot/Ti_3C_2 MXene Nanosheet Composites for Efficient Electrochemical Lithium/Sodium-Ion Storage, *Adv. Energy Mater.*, 2018, **8**, 1801514.

[12] L. Q. Zhu, Z. X. Zhu, J. B. Zhou and Y. T. Qian, Kirkendall effect modulated hollow red phosphorus nanospheres for high performance sodium-ion battery anodes, *Chem. Commun.*, 2020, **56**, 11795-11798.

[13] J. F. Ni, S. D. Fu, C. Wu, Y. Zhao, J. Maier, Y. Yu and L. Li, Superior Sodium Storage in $Na_2Ti_3O_7$ Nanotube Arrays through Surface Engineering, *Adv. Energy Mater.*, 2016, **6**, 1502568.

[14] H. N. He, X. L. Li, D. Huang, J. Y. Luan, S. L. Liu, W. K. Pang, D. Sun, Y. G. Tang, W. Z. Zhou, L. R. He, C. H. Zhang, H. Y. Wang and Z. P. Guo, Electron-Injection-Engineering Induced Phase Transition toward Stabilized 1T-MoS_2 with Extraordinary Sodium Storage Performance, *ACS Nano*, 2021, **15**, 8896-8906.

[15] Y. Jiang, M. Wei, J. K. Feng, Y. C. Ma and S. L. Xiong, Enhancing the cycling

stability of Na-ion batteries by bonding SnS_2 ultrafine nanocrystals on amino-functionalized graphene hybrid nanosheets, *Energy Environ. Sci.*, 2016, **9**, 1430-1438.

[16] H. Gao, J. Z. Niu, C. Zhang, Z. Q. Peng and Z. H. Zhang, A Dealloying Synthetic Strategy for Nanoporous Bismuth-Antimony Anodes for Sodium Ion Batteries, *ACS Nano*, 2018, **12**, 3568-3577.

[17] F. Yang, J. Hong, J. Hao, S. Zhang, G. Liang, J. Long, Y. Liu, N. Liu, W. K. Pang, Ultrathin Few-Layer GeP Nanosheets via Lithiation-Assisted Chemical Exfoliation and Their Application in Sodium Storage, *Adv. Energy Mater.*, 2020, **10**, 1903826.

[18] D. Sun, D. L. Ye, P. Liu, Y. G. Tang, J. Guo, L. Z. Wang and H. Y. Wang, MoS_2/Graphene Nanosheets from Commercial Bulky MoS_2 and Graphite as Anode Materials for High Rate Sodium-Ion Batteries, *Adv. Energy Mater.*, 2018, **8**, 1702383.

[19] F. F. Liu, X. L. Cheng, R. Xu, Y. Wu, Y. Jiang and Y. Yu, Binding Sulfur-Doped Nb_2O_5 Hollow Nanospheres on Sulfur-Doped Graphene Networks for Highly Reversible Sodium Storage, *Adv. Funct. Mater.*, 2018, **28**, 1800394.

[20] M. Q. Zhao, X. Q. Xie, C. E. Ren, T. Makaryan, B. Anasori, G. X. Wang and Y. Gogotsi, Hollow MXene Spheres and 3D Macroporous MXene Frameworks for Na-Ion Storage, *Adv. Mater.*, 2017, **29**, 1702410.

[21] Y. T. Wu, P. Nie, J. M. Jiang, B. Ding, H. Dou and X. G. Zhang, MoS_2-Nanosheet-Decorated 2D Titanium Carbide (MXene) as High-Performance Anodes for

Sodium-Ion Batteries, *Chemelectrochem*, 2017, **4**, 1560-1565.

[22] H. Kim, J. Hong, Y. U. Park, J. Kim, I. Hwang and K. Kang, Sodium Storage Behavior in Natural Graphite using Ether-based Electrolyte Systems, *Adv. Funct. Mater.*, 2015, **25**, 534-541.

[23] B. Cao, H. Liu, B. Xu, Y. F. Lei, X. H. Chen and H. H. Song, Mesoporous soft carbon as an anode material for sodium ion batteries with superior rate and cycling performance, *J. Mater. Chem. A*, 2016, **4**, 6472-6478.

[24] J. Ding, H. L. Wang, Z. Li, A. Kohandehghan, K. Cui, Z. W. Xu, B. Zahiri, X. H. Tan, E. M. Lotfabad, B. C. Olsen and D. Mitlin, Carbon Nanosheet Frameworks Derived from Peat Moss as High Performance Sodium Ion Battery Anodes, *ACS Nano*, 2013, **7**, 11004-11015.